Model reference adaptive damping control for a nanopositioning stage with load uncertainties

Jie Ling (iD), Zhao Feng (iD), Min Ming, and Xiaohui Xiao (iD)

View Online   Export Citation   CrossMark

Model reference adaptive damping control for a nanopositioning stage with load uncertainties

Jie Ling,[1] [iD] Zhao Feng,[1] [iD] Min Ming,[1] and Xiaohui Xiao[1,2,a)] [iD]

AFFILIATIONS

[1] School of Power and Mechanical Engineering, Wuhan University, Wuhan 430072, China
[2] Shenzhen Institute of Wuhan University, Shenzhen 518057, China

[a)] Author to whom correspondence should be addressed: xhxiao@whu.edu.cn.

ABSTRACT

In this paper, a scheme of model reference adaptive integral resonant control (MRAIRC) is presented for adaptive precision motion control of a piezo-actuated nanopositioning platform. The major advantage of the proposed scheme lies in the adaptivity for dynamic changes resulting from load uncertainties. Existing standard integral resonant control (IRC) with constant controller gains is normally designed based on the identified system model under no external load. For the proposed MRAIRC, a standard IRC is first designed using an analytical approach, assuming that a second-order system model is obtained in advance. Afterwards, the designed closed-loop is utilized as a reference model for systems with model uncertainties. The adaptive laws of the controller gains are determined according to the well-known MIT rules. An offline trail-and-error operation is conducted for adaption gains' tuning. The stability of this adaptive control system is proved through Lyapunov stability analysis. Simulation and experimental studies demonstrate that the proposed MRAIRC is superior to the standard IRC in terms of the tracking errors for commonly used raster scanning signals at 5, 10, and 20 Hz with load variations of the platform ranging from 0 to 1000 g.

Published under license by AIP Publishing. https://doi.org/10.1063/1.5064722

I. INTRODUCTION

Piezo-flexure nanopositioning stages are extensively utilized to produce precision motions in many modern scientific instruments or industrial equipment, such as atomic force microscopes (AFMs),[1] high-density data storage,[2] optical measurement,[3] wafer stage,[4] to name a few. Thanks to the merits of rapid response, large output force, and sub-nanometer resolution of piezo actuators,[5–7] along with the superiorities of compact structure, wear-free, and little requirement of maintenance of flexure hinge,[8,9] nanopositioning stages can provide fine mechanical displacements with high-precision and high-resolution. However, an inherent problem that restricts the motion speed is the lightly damped resonance modes owing to the large length-to-diameter ratio of the mechanical construction.[8,10–13] For instance, during raster scanning of AFMs, vibrations will be excited by the input triangular signals which contain frequencies around the lightly damped resonances of the stage.[14] To push the boundaries of nanopositioning performance in terms of speed and accuracy, damping and tracking control algorithms have been widely investigated.

Feedforward damping controllers are designed to compensate for vibrations caused by lightly damped modes, such as inversion-based compensator,[15] modeling-free iterative learning control (ILC),[16] and ILC with linear time-varying (LTV) Q-filters.[7] The main drawback of feedforward approaches lies in the low robustness in the presence of model uncertainties.[10,14,17]

Feedback approaches that control lightly damped vibrational modes and improve overall tracking performance have been developed in the past.[9,12,13,18–22] High-bandwidth damping controllers are designed to tackle the issue of vibrations, such as robust H_∞ control,[20] μ-synthesis,[21] linear-quadratic-Gaussian (LQG) regulator,[22] and sliding mode control. However, the order of such controllers relies heavily on the order of the systems,[10,14] i.e., the design process tends to be complex or inefficient for high-order systems, and the implementation of such controllers will not be economical.

For this, negative-imaginary (NI) feedback damping controllers are designed for vibration control of systems with flexible structures like piezo nanopositioners.[23] For a NI system, a strictly NI controller can be designed to guarantee the internal stability of the positive-feedback interconnection of the two systems.[23,24] These controllers

are fixed-structure, low-order, and ease of implementation, including, but not limited to, positive position feedback (PPF),[25] positive velocity and position feedback (PVPF),[26] positive acceleration, velocity and position feedback (PAVPF),[27] integral force feedback (IFF),[28] passive shunt-damping (PSD),[29] resonant control (RC),[30] recursive delayed position feedback (RDPF),[31] and integral resonant control (IRC).[32–34] Among the above cited studies, IRC is a simple and low-order approach for vibration suppression of systems with multiple resonant modes while maintaining a large stability margin.[34] Consequently, IRC has been widely applied for damping a variety of flexible systems such as a piezoelectric tube,[32] AFMs,[35] a flexible manipulator,[36] precision servomechanism,[37] and so on.

The basic idea of an IRC scheme is adding a constant feed-through term d to the controlled system $G(s)$, so that the modified system $\widehat{G}(s) = G(s) + d$ can be zero-pole interlacing.[32,33] On the basis of this, an integrator $C(s) = k_d/s$ can be utilized in a positive feedback loop to damp the vibrational modes. By tuning the integral gain k_d, a maximum (MAX) damping ratio for the vibrational modes can be achieved. To determine a proper value of the integral gain k_d, designers can apply a trial-and-error approach by plotting the root-locus directly[34] or an analytical approach.[33] The whole design process is based on an identified nominal system model; however, a common system uncertainty is the change of resonance frequency, which may lead to weak performance or even instability of the designed IRC controller.[38,39] Various factors account for the resonance changes, such as surrounding temperature, humidity, atmospheric pressure, and mechanical loads.[38] For this, adaptive feedback damping control is necessary for robust vibration attenuation of nanopositioners in the presence of system uncertainty.

The motivation of this paper is to design a model reference adaptive integral resonant controller (MRAIRC) by applying a model reference adaptive control approach into the standard IRC scheme to deal with resonance changes caused by mechanical loading variations. First, a standard IRC is designed for an identified nominal system with no load using the analytical approach in Ref. 33. Then, the designed closed-loop is utilized as a reference model for systems with model uncertainty. The adaptive laws of the controller gains are chosen according to the well-known MIT rules.[40] The stability of this adaptive control system is demonstrated according to a Lyapunov stability criterion. The proposed model reference adaptive IRC is also implemented with experimental verification on a piezo nanopositioner in this paper.

The experimental setup and system identification are described in Sec. II. A brief introduction for a standard IRC design using analytical approach is presented in Sec. III. Then, the proposed model reference adaptive IRC is discussed in Sec. IV. The experimental results that verify the expected improvements in positioning precision are presented in Sec. V. The conclusions are given in Sec. VI.

II. EXPERIMENTAL SETUP AND SYSTEM IDENTIFICATION

A. Experimental setup

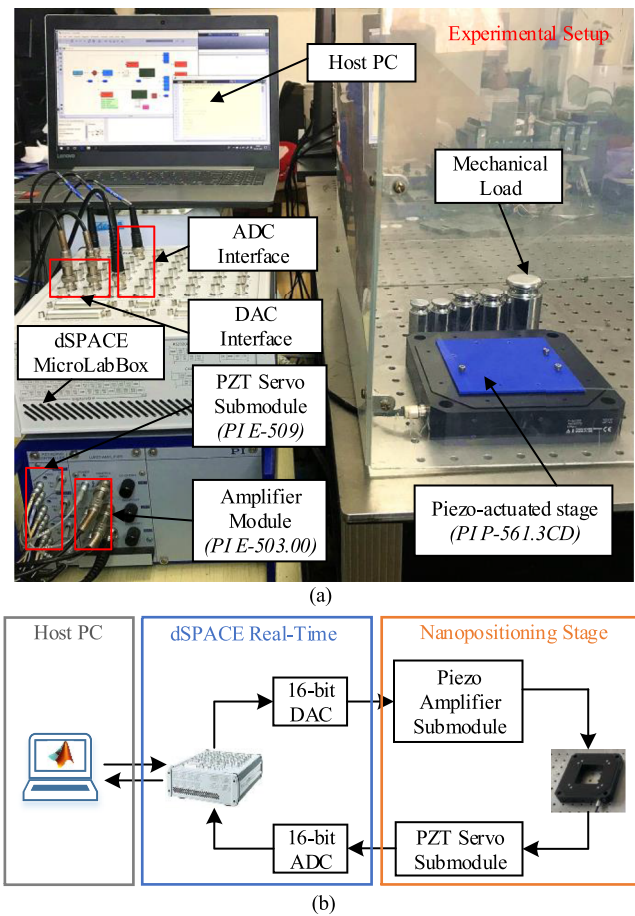The experimental setup utilized in this work is shown in Fig. 1. A commercial three-axis piezoelectric nanopositioning

FIG. 1. The experimental setup of a piezo-actuated nanopositioning system: (a) experimental platform and (b) block diagram of signal flow.

platform (model: P-561.3CD, Physik Instrumente Co., Ltd.) is employed in this paper for the verification of the proposed control strategy.

The signal flow of the control system is described in Fig. 1(b). For each axis, the control input voltage in the range of 0–10 V is produced by 16-bit digital to analog interfaces (DACs) of the data output module in a real-time controller (model: MicroLabBox, dSPACE Co., Ltd.). A piezo amplifier module (model: E-503.00, Physik Instrumente Co., Ltd.) with a fixed gain of 10 amplifies the input voltage and generates the excitation voltage between 0 and 100 V. The output of each motion axis with a stroke of 100 μm, which is read by a piezoelectric transducer (PZT) servo submodule (model: E-509.C3A, Physik Instrumente Co., Ltd.), is subsequently passed to the data input module in dSPACE MicroLabBox with 16-bit analog to digital interfaces (ADCs). The control algorithm is designed in MATLAB®/Simulink block diagram on the host personal computer (PC) and then downloaded and executed on the target dSPACE MicroLabBox in the real-time software environment of dSPACE ControlDesk.

It should be noted that, in this work, only the y-axis was used to implement the proposed controller of adaptive damping for

single-input-single-output (SISO) systems, and the sampling frequency of the system was set to 10 kHz.

B. System identification

In this section, a nominal system model under no mechanical load and a set of perturbed system model under load variations between 200 and 1000 g were identified for controller design as well as the simulation studies before experimental implementation.

1. Nominal system

A sine-sweep input voltage with a constant amplitude of 200 mV between 0.1 Hz and 500 Hz was applied to the y-axis. A low magnitude of input voltage was used here to avoid distortion from hysteresis.[41] The dynamic model of the nominal system with no mechanical load is obtained using the Identification Toolbox of MATLAB, which can be represented as

$$G(s) = \frac{y(s)}{u(s)} = \frac{1.198 \times 10^6}{s^2 + 110s + 1.673 \times 10^6}, \qquad (1)$$

where $u[V]$ is the input driving voltage and $y[\mu m]$ is the output displacement.

As depicted in Fig. 2, the identified and measured frequency responses indicate that Eq. (1) captures the dynamics of the platform well between the frequency range of 1–400 Hz. It should be noted that the hysteresis nonlinearity is regarded as input disturbances, which can be alleviated by a high-gain feedback controller in the following damping controller scheme.[31] Taking a close look at Fig. 2, it can be observed that the first resonant mode of the system with no loaded mass occurs at the frequency of 205 Hz with
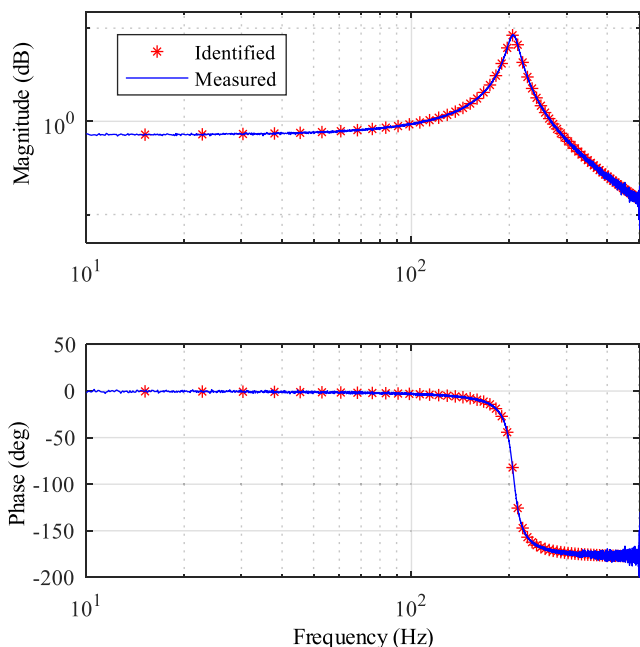
a magnitude of 18.5 dB, where the damping controller is needed to be designed to reject the unexpected vibrations.

2. Perturbed system

Using the same method as said above, a set of system identifications was conducted to obtain the perturbed models under different loads. The identified system models are displayed in Fig. 3. On the one hand, with the increase in mechanical loads, the position of the first resonance shifts to the left along the frequency axis with the decrease in the corresponding magnitude of the resonance peak; on the other hand, minor changes occur in the overall system gain at lower frequencies compared with the resonance frequency.

To be specific, the resonance frequency shifts from 205 Hz to 98.4 Hz with the change of magnitude from 18.5 dB to −1.73 dB under the mechanical load variations from 0 to 1000 g. It can be seen that variations in mechanical loads have a pronounced impact on the system dynamics at the resonance frequency. This may lead to weakened performance or even divergence of a damping controller designed based on the nominal system dynamics with no load. Hereto, the adaptivity of damping controllers is necessary for dealing with mechanical load variations.

Remark 1. The purpose of the perturbed system identification is twofold. First, it is performed to reveal that the resonant frequency shifts under load variations instead of staying still. Second, the perturbed models will be utilized to test the controllers' performance under load induced uncertainties in Sec. V. However, it does not mean that the load variation as well as the induced uncertainty is fixed. Actually, in some applications of microassembling or AFM

FIG. 2. Comparisons of the Bode diagram of measured results and identified results.
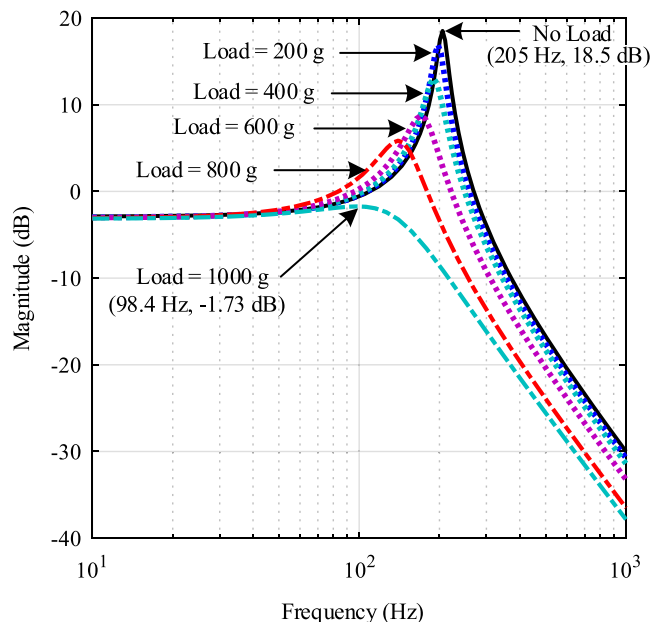
FIG. 3. Bode diagrams of the identified perturbed models under mechanical load variations.

scanning, the load variation has a relatively certain range rather than a specific value. For this, the designed controller should perform consistently in this variation range, which is the purpose of adaptive damping controller design in this work.

III. STANDARD IRC SCHEME

A brief review of the standard IRC design using the analytical approach is reviewed in this section. Readers may refer to Refs. 33 and 34 for details.

The dominant dynamics of a piezoelectric nanopositioning stage with a lightly damped mode can be given as a second-order system

$$G(s) = \frac{y(s)}{u(s)} = \frac{\sigma^2}{s^2 + 2\xi_n \omega_n s + \omega_n^2}, \quad (2)$$

where s is the Laplace operator, $y[\mu m]$ and $u[V]$ are the output displacement and the input driving voltage, respectively, σ^2 is the system gain in low frequencies, and ξ_n and ω_n are the damping coefficient and the natural frequency of the plant, respectively. For a piezoelectric nanopositioning system, $\xi_n \ll 1$, which indicates that the resonant mode at ω_n is lightly damped.

As shown in Fig. 4, the standard IRC consists of two loops, i.e., an inner positive feedback loop for damping vibrations and an outer negative loop for improving the tracking accuracy. In the damping loop, a feedforward term d is added to produce a pair of zeros z_1, z_2 = $\pm j\omega_z$ which satisfies $\omega_n/3 < \omega_z < \omega_n$. The term d can be calculated as

$$d = -2\frac{\sigma^2}{\omega_n^2} \triangleq -2d_c, \quad (3)$$

where d_c represents the DC gain of the system in Eq. (1).

The damping loop T_{damp} is defined from the output of the tracking controller y_{track} to the measured system output y as

$$T_{damp}(s) \triangleq \frac{C_{damp}(s) \cdot G(s)}{1 - C_{damp}(s) \cdot \widehat{G}(s)}, \quad (4)$$

where $\widehat{G}(s) = G(s) + d$ stands for the modified system by the feedthrough term d.

The damping controller gain k_d is found to maximize the damping ratio of the damping loop. The achievable maximum damping ratio can be obtained by

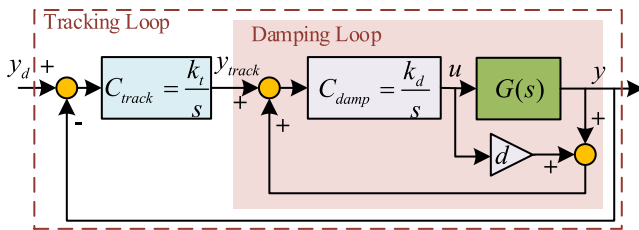$$\xi_{max} = \frac{1}{2}\left(\frac{\omega_n}{\sqrt{\omega_n^2 + \sigma^2/d}} - 1\right), \quad (5)$$

with the corresponding damping controller gain chosen by

$$k_d|_{\xi_{max}} = \frac{1}{|d|}\left(\omega_n \cdot \sqrt{\frac{\omega_n}{\sqrt{\omega_n^2 + \sigma^2/d}}}\right). \quad (6)$$

Regarding the tracking controller, the gain is tuned so that

$$k_t \cdot k_d < -\frac{\sigma^2 + d \cdot \omega_n^2}{d^2}. \quad (7)$$

Remark 2. As can be seen from Fig. 3, change of ω_n is induced by load variation, which demands a corresponding adaptivity for k_d by Eq. (6) as well as for k_t by Eq. (7). However, in the determination process of a standard IRC scheme, k_d and k_t are fixed once chosen. Therefore, system uncertainties caused by mechanical load variations is not considered in the conventional design processes either by the trial-and-error approach or by the analytical approach. For this, the adaptivity of the standard IRC has room for improvements.

IV. PROPOSED MRAIRC SCHEME

Section III describes the design of a standard IRC with constant controller gains k_t and k_d. In practice, mechanical load variations cause resonance changes. To deal with this issue, the basic idea of MRAIRC is to implement an adaptive damping controller with parameters updated online to change the closed-loop system dynamics.

A. MRAIRC controller design

The control structure of a MRAIRC system is shown in Fig. 5. $\widetilde{C}_{track}$ and $\widetilde{C}_{damp}$ represent the designed adaptive tracking and damping controllers with automatically adjusted gains, respectively, which are different from C_{track} and C_{damp} with constant gains in Fig. 4. Two reference models $M_{damp}(s)$ and $M_{track}(s)$ are chosen to generate the desired trajectories for the inner damping loop output and the outer tracking loop output, respectively. The control errors
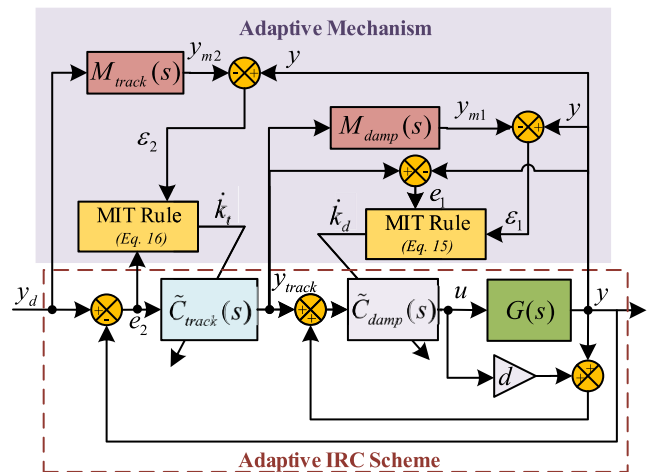

FIG. 4. Standard IRC scheme.

FIG. 5. Block diagram of the proposed MRAIRC.

ε_1 and ε_2 are defined as the deviation of the system output y from the reference models' outputs y_{m1} and y_{m2}. The adaptive adjustment mechanism automatically adjusts the controller parameters k_d and k_t so that the closed-loop control system's outputs follow that of the reference models. The reference models are chosen based on the designed damping loop and tracking loop with no mechanical loads according to the method in Sec. III

$$M_{damp}(s) = \frac{C_{damp}(s) \cdot G(s)}{1 - C_{damp}(s) \cdot \widehat{G}(s)} \tag{8}$$

and

$$M_{track}(s) = \frac{C_{track}(s) \cdot C_{damp}(s) \cdot G(s)}{1 - C_{damp}(s)\widehat{G}(s) + C_{track}(s)C_{damp}(s)G(s)}, \tag{9}$$

where $G(s)$ is the identified nominal system with no mechanical loads, $C_{damp}(s)$, $C_{track}(s)$, and $\widehat{G}(s)$ are designed using the analytical approach in Eqs. (3), (6), and (7). In Fig. 5, both the adjustment mechanisms for generating $\dot{k}_d$ and $\dot{k}_t$ adopt the same MIT rule. For this, the derivation process for $\dot{k}_d$ is discussed below for instance.

Considering the control error

$$\varepsilon_1 = y - y_{m1}, \tag{10}$$

a cost function is denoted as

$$J = \frac{1}{2}\varepsilon_1^2. \tag{11}$$

According to the so-called MIT rule,[40] the adaptive law of k_d can be obtained as follows:

$$\begin{aligned} \dot{k}_d &= -\gamma_d \cdot \frac{\partial J}{\partial k_d} \\ &= -\gamma_d \cdot \frac{\partial J}{\partial \varepsilon_1} \cdot \frac{\partial \varepsilon_1}{\partial y} \cdot \frac{\partial y}{\partial k_d} \\ &= -\gamma_d \cdot \varepsilon_1 \cdot \frac{\partial y}{\partial k_d}, \end{aligned} \tag{12}$$

where γ_d is known as the adaption gain and the component of $\frac{\partial y}{\partial k_d}$ is the sensitivity derivative of the system output with respect to the controller gain k_d.

The damping loop function in Eq. (4) can be expanded as

$$\frac{y(s)}{y_{track}(s)} = \frac{k_d \cdot \sigma^2}{s^3 + (2\xi_n\omega_n - k_d d)s^2 + (\omega_n^2 - 2\xi_n\omega_n k_d d)s - k_d(\sigma^2 + d\omega_n^2)}, \tag{13}$$

from which $\frac{\partial y}{\partial k_d}$ can be derived by

$$\frac{\partial y}{\partial k_d} = \frac{\sigma^2 \cdot (y - y_{track})}{\nabla^3 + (2\xi_n\omega_n - k_d d)\nabla^2 + (\omega_n^2 - 2\xi_n\omega_n k_d d)\nabla - k_d(\sigma^2 + d\omega_n^2)}, \tag{14}$$

where the differential operator $\nabla \triangleq d/dt$. To converge to the reference model (i.e., $y_{m1} = y$ in Fig. 5), an approximate operation can be made by substituting the parameters in the denominator of Eq. (14)

by the corresponding parts in the denominator of the model M_{damp} in Eq. (8). Hereto, the adaptive law of k_d can be achieved as

$$\dot{k}_d = \gamma_d \cdot \varepsilon_1 \cdot e_1 \cdot \frac{\sigma^2}{\nabla^3 + a_{m2}\nabla^2 + a_{m1}\nabla + a_{m0}}, \tag{15}$$

where the parameters $\{a_{m0}, a_{m1}, a_{m2}\}$ are the coefficients of the terms $\{s^0, s^1, s^2\}$ in the denominator of the reference model in Eq. (8) and the tracking error is defined as $e_1 = y_{track} - y$.

Similarly, the adaptive law of k_t can be derived as

$$\dot{k}_t = \frac{\gamma_t \cdot \varepsilon_2 \cdot e_2 \cdot k_d \cdot \sigma^2}{\nabla^4 + a_{n3}\nabla^3 + a_{n2}\nabla^2 + a_{n1}\nabla + a_{n0}}, \tag{16}$$

where γ_t is the adaption gain for tracking controller, control error $\varepsilon_2 = y - y_{m2}$, tracking error $e_2 = y_d - y$, and the parameters $\{a_{n0}, a_{n1}, a_{n2}, a_{n3}\}$ are the coefficients of the terms $\{s^0, s^1, s^2, s^3\}$ in the denominator of the reference model M_{track} in Eq. (9). It should be noted that k_d should be calculated in advance so that k_t can be obtained through Eq. (16). Stability proof for the proposed MRAIRC scheme can be found in Appendix A.

Remark 3. The adaptive laws in Eqs. (15) and (16) have two parameters, the adaption gain γ_d and γ_t, which need to be chosen by the controller designer. Generally, the two adaption gains can be determined by a trial-and-error approach[40] with the aid of convergence diagrams of the parameters in simulations.

B. Overall design procedure

As illustrated in Fig. 5, the proposed MRAIRC consists of two reference model loops, and each loop has an adaption gain to be tuned for parameter's convergence. For the convenience of designers, the overall design procedure for the proposed MRAIRC is summarized as follows:

Step (1): Identify the nominal system as well as the perturbed system with load uncertainties, as shown in Figs. 2 and 3.
Step (2): Design the standard IRC based on the nominal system model and choose the controller parameters according to Eqs. (3), (6), and (7).
Step (3): Design MRAIRC, as in Fig. 5, using Eqs. (15) and (16). The reference models of M_{damp} and M_{track} are chosen as the designed damping loop and tracking loop in Step 2.
Step (4): Determine the adaptation gains γ_d and γ_t through trial-and-error to obtain a satisfied adaptation rate for parameters k_d and k_t.
Step (5): Evaluate the designed controller through simulations and experiments.
Step (6): Stop.

It can be seen from the overall design procedure that only two parameters γ_d and γ_t need to be determined by the designer, which simplifies the design process.

V. EVALUATIONS AND DISCUSSIONS

In this section, the effectiveness of the proposed MRAIRC scheme is demonstrated through conducting a series of simulations and experiments on the piezoelectric nanopositioning stage mentioned in Fig. 1.

A. Controller design results

As stated in the overall design procedure, a standard IRC needs to be designed before the MRAIRC. In this paper, IRC is also used for the comparative controller in simulations and experiments.

1. IRC

According to Eqs. (3), (6), and (7), a standard IRC is designed first on the basis of an identified nominal system in Eq. (1). The designed IRC is

$$d = -1.43, \quad C_d = \frac{1098}{s}, \quad \text{and } C_t = \frac{258}{s}. \tag{17}$$

2. MRAIRC

On the basis of Eq. (17), the reference models for the damping loop and the tracking loop are chosen as

$$
\begin{aligned}
M_{damp} &= \frac{1.286 \times 10^9}{s^3 + 1648s^2 + 1.842 \times 10^6 s + 1.286 \times 10^9}, \\
M_{track} &= \frac{3.847 \times 10^{11}}{s^4 + 1648 \times s^3 + 1.842 \times 10^6 s^2} \\
&\quad + 1.286 \times 10^9 s + 3.847 \times 10^{11}.
\end{aligned}
\tag{18}
$$

Then, the adaptation laws of controller parameters k_d and k_t are

$$
\begin{aligned}
\dot{k}_d &= \frac{\gamma_d \cdot \varepsilon_1 \cdot e_1 \cdot 1.198 \times 10^6}{\nabla^3 + 1648\nabla^2 + 1.842 \times 10^6 \nabla + 1.286 \times 10^9}, \\
\dot{k}_t &= \frac{\gamma_t \cdot \varepsilon_2 \cdot e_2 \cdot k_d \cdot 1.198 \times 10^6}{\nabla^4 + 1648 \times \nabla^3 + 1.84 \times 10^6 \nabla^2} \\
&\quad + 1.29 \times 10^9 \nabla + 3.85 \times 10^{11},
\end{aligned}
\tag{19}
$$

where the unknown gains γ_d and γ_t need to be tuned and determined through a trial-and-error approach by plotting the adaption process of parameters k_d and k_t.

Recalling Fig. 5, the controlled plant $G(s)$ was set as a nominal system model, and the reference models were set as Eq. (18). It was expected that the controller parameters k_d and k_t should converge to the ideal values in Eq. (17) under certain γ_d and γ_t. By tuning the adaption gains, the designed results are shown in Fig. 6. It can be seen that the controller parameters converge to the responding ideal values (i.e., $k_d \to 1098$ and $k_t \to 258$) as the system output approaches the steady state. Finally, the designed adaption gains are

$$\gamma_d = -8.4 \times 10^9, \quad \gamma_t = -1.2 \times 10^9. \tag{20}$$

B. Simulations

Before experiments, simulations were conducted to test the tracking performance as well as the stability of the designed controller. The results of 10 Hz raster tracking with IRC and MRAIRC controllers are displayed together for comparisons in Fig. 7. The controlled plant was the identified model under the 1000 g mechanical load as shown in Fig. 3. It should be noted that a segment of zeros (0.2 s) was fed into the platform in advance before the raster signals so that the controller gains could have enough time to converge to steady states as mentioned in Fig. 6. To compare the tracking performances of the two controllers, the phase lags of the recorded system outputs were removed as perfectly delayed tracking was better
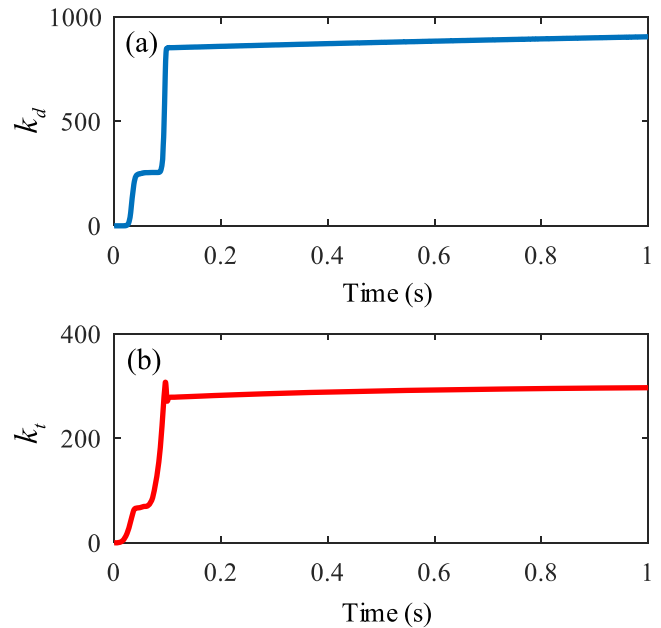

FIG. 6. Adaption process of the MRAIRC controller parameters: (a) damping controller gain k_d and (b) tracking controller gain k_t.

than imperfect timely tracking in AFM applications.[31] The shifted outputs $y_d(t - k^* t_s)$ can be obtained with the delayed term k^* calculated as
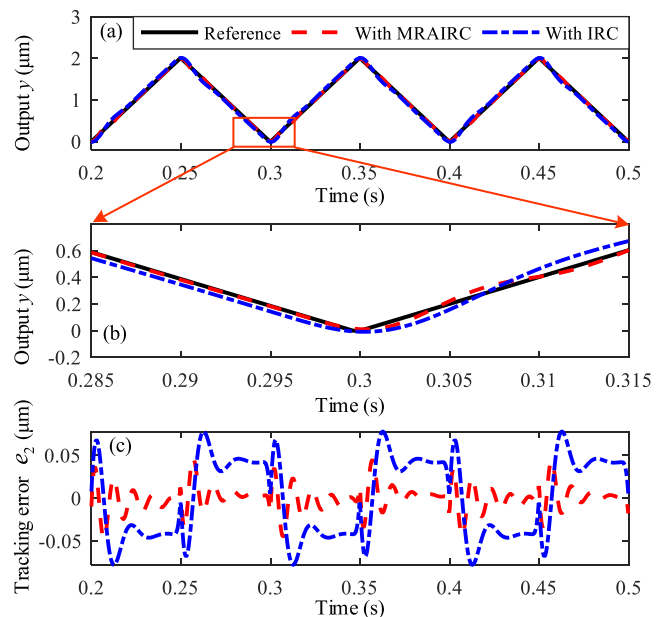

FIG. 7. Simulation results of 10 Hz raster tracking under a 1000 g load with IRC and MRAIRC: (a) overall tracking view, (b) partial enlarged view of the red box marked part in (a), and (c) overall tracking errors.

$$k^* = \arg \min_{k} \max_{t \in [0, 2T]} |y_d(t - kt_s) - y(t)|, \quad (21)$$

where T is denoted as the period of the input reference and t_s is the sampling time interval of the control system.

To compare the two controllers' performance quantificationally, the root-mean-square error (RMS) and maximum (MAX) error were adopted as the performance indexes in this paper for evaluations denoted as

$$e_{max} = \max_{t \in [T_a, T_b]} (y_d(t - k^* t_s) - y(t)),$$

$$e_{rms} = \sqrt{\frac{1}{(T_b - T_a)/t_s} \sum_{t=T_a}^{T_b} (y_d(t - k^* t_s) - y(t)),} \quad (22)$$

where the evaluated signals last from T_a to T_b.

In Fig. 7, it can be intuitively observed that the output trajectory tracks input reference more closely and steadily with the proposed MRAIRC controller than with the traditional IRC controller. To be more specific, the IRC controller produces the MAX and RMS values of tracking errors e_2 (see Fig. 5) of 0.078 and 0.047 μm, which account for 3.9% and 2.3% of the tracking range, respectively. By contrast, the proposed MRAIRC controller generates the MAX and RMS errors of 0.048 and 0.015 μm, which make improvements of 40% and 67% over that of the IRC controller. More case studies and analysis are presented in the following section.
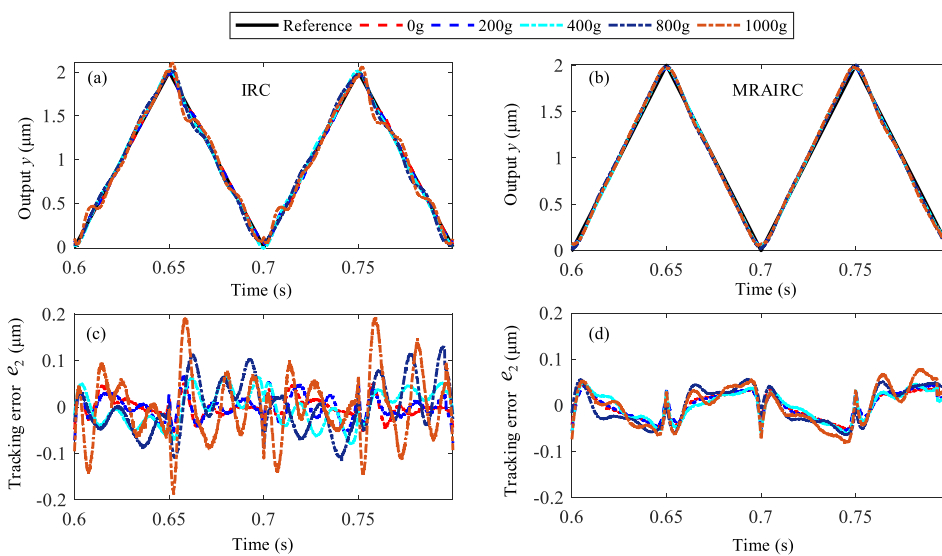
C. Experiments

In the experimental cases, the IRC controller was also implemented for a comparative study with the proposed MRAIRC. Considering that the first resonant frequency of the nanopositioning stage occurs at 205 Hz as displayed in Fig. 2, a set of raster references at 5 Hz, 10 Hz, and 20 Hz was fed into the system. With respect to the mechanical loads, a set of load variations at 0 g, 200 g, 400 g, 800 g,

and 1000 g was chosen for testing the controllers under dynamics uncertainties. The results are shown in Figs. 8 and 9.

Figure 8 indicates that, with increasing loaded mass, the performance of standard IRC tends to deteriorate with a distinct increase of tracking errors. For the proposed MRAIRC controller, the tracking performances under different loads are consistent with little variations when compared with IRC, which implies that the closed-loop control system with MRAIRC is less sensitive to load variation induced uncertainties. Moreover, the magnitudes of tracking errors are generally smaller with the MRAIRC controller than those with the IRC controller. Taking a quantitative view of the results, the RMS and MAX errors of MRAIRC under 0–1000 g range from 0.025 to 0.046 μm and from 0.059 to 0.074 μm, respectively. However, for the IRC controller, the corresponding RMS and MAX errors range from 0.025 to 0.080 μm and from 0.054 to 0.171 μm. It can be found that for a 0 g load, the two controllers produce close performance. With the increase in load uncertainties, the RMS and MAX errors of MRAIRC increased to 0.021 and 0.015 μm, while the two indexes' changes are 0.055 and 0.117 μm for IRC, which are 2.6 and 7.8 times than those of MRAIRC.

The whole statistical results of RMS and MAX errors of the experimental data are displayed in Fig. 9 for intuitive comparisons of IRC and MRAIRC. For the 5 Hz raster tracking, both the controllers performed steadily versus dynamic uncertainties. When the input raster reached 20 Hz, both the controllers resulted in larger errors than the corresponding cases of 5 Hz raster tracking. However, the MRAIRC's performance was still more consistent for dynamic uncertainties than that of IRC. The maximum MAX and RMS errors for IRC occurred in the case of 20 Hz raster tracking with a 1000 g load, which were 0.368 and 0.211 μm as large as 18% and 11% of the positioning range, respectively. This was one of the reasons why 20 Hz was the maximum chosen input frequency for the experimental studies. The maximum MAX and RMS errors for MRAIRC occurred similarly in the case of 20 Hz raster tracking with a 1000 g load. They were 0.176 and 0.097 μm, which were also much smaller than those of IRC. Herein, the experimental results

FIG. 8. Experimental results of 10 Hz raster tracking under a 0–1000 g load with IRC and MRAIRC [(a) and (c) are the overall tracking view and the corresponding tracking errors of IRC; (b) and (d) are those of MRAIRC].
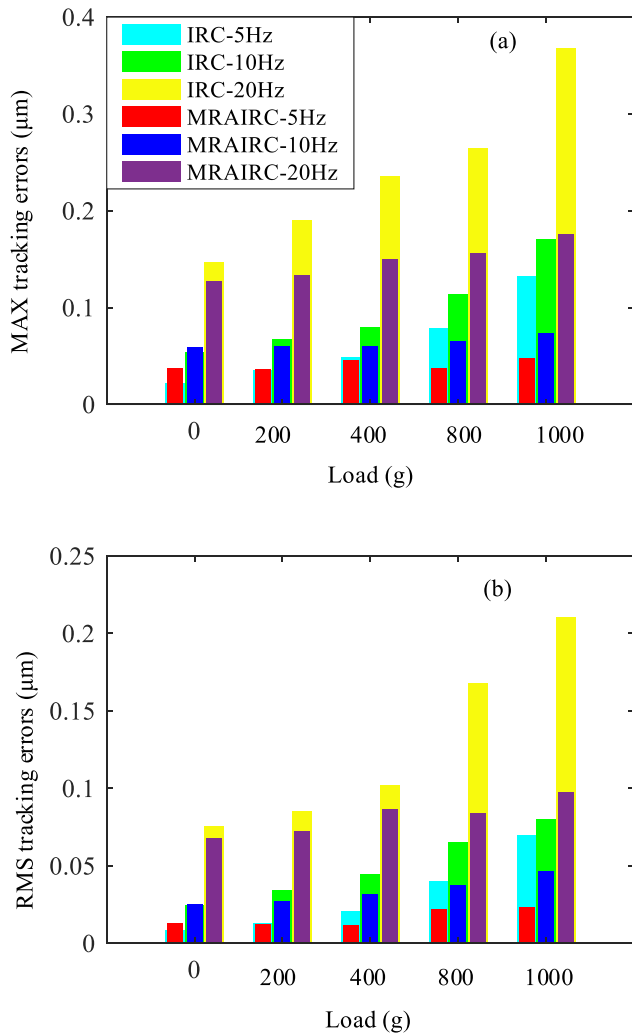
FIG. 9. Tracking errors of 5 Hz, 10 Hz, and 20 Hz raster signals under a 0–1000 g load with IRC and MRAIRC:(a) MAX errors and (b) RMS errors.

generally demonstrated that the proposed MRAIRC performed better than the IRC for 5–20 Hz raster tracking with load variations from 0 to 1000 g.

D. Discussions

The foregoing experimental results verified the effectiveness and adaptivity of the reported MRAIRC scheme for precision motion control of piezoelectric nanopositioners with load uncertainties. As mentioned earlier, this paper focuses on the vibration control issue for lightly damped modes caused by flexible hinges of piezoelectric nanopositioners rather than the issue of hysteresis and creep nonlinearities. For this, the references to be tracked are limited within 2 μm, which occupies 2% of the overall displacement stroke of the motion axis. As a future work, hysteresis of nanopositioners may be considered for adaptive damping control versus load variations.

It is also notable that concerning the proposed MRAIRC scheme, the adaption gains γ_d and γ_t are tuned offline by a trial and error approach to achieve ideal adaption rates. From a theoretical point of view, the adaption gains can be chosen approximately instead of optimally at the cost of slower adaption processes, which can simplify the work of designers.

VI. CONCLUSIONS

A novel MRAIRC scheme has been reported for adaptive precision motion control for piezoelectric nanopositioners in this paper. First, a standard IRC needs to be designed for an identified nominal system with no load using the analytical approach. Then, the designed closed-loop is utilized as a reference model for systems with model uncertainty. The adaptive gains of the controller are chosen according to the well-known MIT rules. The stability of this adaptive control system is demonstrated according to a Lyapunov method. Both simulations and experiments are conducted based on a piezo nanopositioning platform. The results verify the effectiveness and adaptivity of the proposed MRAIRC controller with comparisons with the standard IRC.

Future works will seek to tackle the issues of hysteresis and vibration simultaneously for adaptive tracking control in the applications of large range scanning for piezo nanopositioners. For this, there is some room for the performance enhancement of the proposed MRAIRC.

APPENDIX A: STABILITY PROOF OF MRAIRC

In this section, the stability proof from input y_{track} to output y of the damping loop is conducted. A similar process can be operated for the tracking loop from input y_d to output y.

Considering the damping loop in Eq. (4) as a mass-spring-damper system, the dynamics model can be rewritten as

$$\dddot{y} + a_2\ddot{y} + a_1\dot{y} + a_0 y = b_0 \cdot y_{track}, \tag{A1}$$

where $\{a_2, a_1, a_0, b_0\}$ are the model coefficients. A reference model for damping loop is chosen as Eq. (8), which can also be developed in the form

$$\dddot{y}_{m1} + a_{m2}\ddot{y}_{m1} + a_{m1}\dot{y}_{m1} + a_{m0}y_{m1} = b_{m0} \cdot y_{track}, \tag{A2}$$

where $\{a_{m2}, a_{m1}, a_{m0}\}$ are consistent with that of Eq. (15) and b_{m0} is the coefficient in the numerator of Eq. (8).

Subtracting Eq. (A2) from Eq. (A1) results in a control error dynamics equation

$$\dddot{\varepsilon}_1 + a_{m2}\ddot{\varepsilon}_1 + a_{m1}\dot{\varepsilon}_1 + a_{m0}\varepsilon_1 = (b_0 - b_{m0})y_{track} + (a_{m2} - a_2)\ddot{y}$$
$$+ (a_{m1} - a_1)\dot{y} + (a_{m0} - a_0)y. \tag{A3}$$

Choosing the error vector as $\mathbf{E} = \begin{bmatrix} \varepsilon_1 & \dot{\varepsilon}_1 & \ddot{\varepsilon}_1 \end{bmatrix}^T$, Eq. (A3) can be restructured in a state-space form as

$$\dot{\mathbf{E}} = \mathbf{A}\mathbf{E} + \beta \mathbf{B} y_{track} + \boldsymbol{\Delta}, \qquad (A4)$$

with

$$\mathbf{A} = \begin{bmatrix} 0 & 1 & 0 \\ 0 & 0 & 1 \\ -a_{m0} & -a_{m1} & -a_{m2} \end{bmatrix}, \quad \mathbf{B} = \begin{bmatrix} 0 \\ 0 \\ 1 \end{bmatrix}, \quad \boldsymbol{\Delta} = \begin{bmatrix} 0 \\ 0 \\ \delta \end{bmatrix},$$

where $\delta = (a_{m2} - a_2)\ddot{y} + (a_{m1} - a_1)\dot{y} + (a_{m0} - a_0)y$ and $\beta = b_0 - b_{m0}$.

A Lyapunov function candidate is considered as

$$V = \frac{1}{2}\mathbf{E}^T\mathbf{P}\mathbf{E}, \qquad (A5)$$

where $\mathbf{P}$ is a symmetric positive definite matrix that satisfies the Lyapunov linear equation

$$\mathbf{A}^T\mathbf{P} + \mathbf{P}\mathbf{A} = -\mathbf{Q}, \qquad (A6)$$

with $\mathbf{Q}$ given as a symmetric positive definite matrix.

In view of Eq. (A4), the time derivative of V can be expressed as

$$\begin{aligned} \dot{V} &= \mathbf{E}^T\mathbf{P}\dot{\mathbf{E}} \\ &= \mathbf{E}^T\mathbf{P}\mathbf{A}\mathbf{E} + \mathbf{E}^T\mathbf{P}(\beta \mathbf{B} y_{track} + \delta) \\ &= \frac{1}{2}\mathbf{E}^T(\mathbf{A}^T\mathbf{P} + \mathbf{P}\mathbf{A})\mathbf{E} + \mathbf{E}^T\mathbf{P}\mathbf{B}(\beta y_{track} + \delta) \\ &= -\frac{1}{2}\mathbf{E}^T\mathbf{Q}\mathbf{E} + \mathbf{E}^T\mathbf{P}\mathbf{B}(\beta y_{track} + \delta). \end{aligned} \qquad (A7)$$

Recalling Eqs. (A1) and (A2), β and δ can be obtained as

$$\begin{aligned} \beta y_{track} + \delta &= \beta \frac{\dddot{y} + a_2\ddot{y} + a_1\dot{y} + a_0 y}{b_0} + (a_{m2} - a_2)\ddot{y} + (a_{m1} - a_1)\dot{y} \\ &\quad + (a_{m0} - a_0)y_1 \\ &= \left(1 - \frac{b_{m0}}{b_0}\right)\dddot{y} + \left(a_{m2} - \frac{b_{m0}}{b_0}a_2\right)\ddot{y} + \left(a_{m1} - \frac{b_{m0}}{b_0}a_1\right)\dot{y} \\ &\quad + \left(a_{m0} - \frac{b_{m0}}{b_0}a_0\right)y \\ &= b_{m0} \cdot y_{track} - \frac{b_{m0}}{b_0} \cdot b_0 \cdot y_{track} = 0. \end{aligned} \qquad (A8)$$

Hence,

$$\dot{V} = -\frac{1}{2}\mathbf{E}^T\mathbf{Q}\mathbf{E} \le 0. \qquad (A9)$$

Hereto, the stability of the damping loop from the input y_{track} to the output y is proved.

REFERENCES

[1]Z. Feng, J. Ling, M. Ming, and X. H. Xiao, "A model-data integrated iterative learning controller for flexible tracking with application to a piezo nanopositioner," Trans. Inst. Meas. Control **40**, 3201–3210 (2018).

[2]A. Sebastian, A. Pantazi, H. Pozidis, and E. Elefthriou, "Nanopositioning for probe-based data storage," IEEE Control Syst. **28**, 26–35 (2008).

[3]D. Kang and D. Gweon, "Development of flexure based 6-degrees of freedom parallel nano-positioning system with large displacement," Rev. Sci. Instrum. **83**, 035003 (2012).

[4]H. P. Shin and J. H. Moon, "Static and dynamic analyses of a 6-DOF ultra-precision parallel mechanism," Int. J. Precis. Eng. Manuf. **19**, 1019–1026 (2018).

[5]M. Rakotondrabe, "Multivariable classical Prandtl-Ishlinskii hysteresis modeling and compensation and sensorless control of a nonlinear 2-DOF piezoactuator," Nonlinear Dyn. **89**, 481–499 (2017).

[6]M. Ming, J. Ling, Z. Feng, and X. H. Xiao, "A model prediction control design for inverse multiplicative structure based feedforward hysteresis compensation of a piezo nanopositioning stage," Int. J. Precis. Eng. Manuf. **19**, 1699–1708 (2018).

[7]Z. Feng, J. Ling, M. Ming, and X. H. Xiao, "High-bandwidth and flexible tracking control for precision motion with application to a piezo nanopositioner," Rev. Sci. Instrum. **88**, 085107 (2017).

[8]Y. K. Yong, S. R. Moheimani, B. J. Kenton, and K. K. Leang, "Invited review article: High-speed flexure-guided nanopositioning: Mechanical design and control issues," Rev. Sci. Instrum. **83**, 121101 (2012).

[9]G. Y. Gu, L. M. Zhu, C. Y. Su, H. Ding, and S. Fatikow, "Modeling and control of piezo-actuated nanopositioning stages: A survey," IEEE Trans. Autom. Sci. Eng. **13**, 313–332 (2016).

[10]J. Ling, Z. Feng, M. Ming, and X. H. Xiao, "Damping controller design for nanopositioners: A hybrid reference model matching and virtual reference feedback tuning approach," Int. J. Precis. Eng. Manuf. **19**, 13–22 (2018).

[11]Z. Feng, J. Ling, M. Ming, and X. H. Xiao, "Data-based double-feedforward controller design for a coupled parallel nanopositioning stage," Proc. Inst. Mech. Eng., Part I **231**, 881–892 (2017).

[12]M. Ming, Z. Feng, J. Ling, and X. H. Xiao, "Hysteresis modelling and feed-forward compensation of piezoelectric nanopositioning stage with a modified Bouc-Wen model," IET Micro Nano Lett. **13**, 1170–1174 (2018).

[13]M. S. Rana, H. R. Pota, and I. R. Petersen, "A survey of methods used to control piezoelectric tube scanners in high speed AFM imaging," Asian J. Control **20**, 1379–1399 (2018).

[14]S. K. Das, H. R. Pota, and I. R. Petersen, "Damping controller design for nanopositioners: A mixed passivity, negative-imaginary, and small-gain approach," IEEE/ASME Trans. Mechatronics **20**, 416–426 (2015).

[15]K. K. Leang, Q. Zou, and S. Devasia, "Feedforward control of piezoactuators in atomic force microscope systems," IEEE Control Syst. **29**, 70–82 (2009).

[16]K. S. Kim and Q. Zou, "A modeling-free inversion-based iterative feedforward control for precision output tracking of linear time-invariant systems," IEEE/ASME Trans. Mechatronics **18**, 1767–1777 (2013).

[17]S. R. Moheimani, "Invited review article: Accurate and fast nanopositioning with piezoelectric tube scanners: Emerging trends and future challenges," Rev. Sci. Instrum. **79**(7), 071101 (2008).

[18]A. A. Eielsen, M. Vagia, J. T. Gravdahl, and K. Y. Pettersen, "Damping and tracking control schemes for nanopositioning," IEEE/ASME Trans. Mechatronics **19**, 432–444 (2014).

[19]I. R. Petersen, "Negative imaginary systems theory and applications," Annu. Rev. Control **42**, 309–318 (2016).

[20]O. Aljanaideh and M. Rakotondrabe, "Observer and robust h-INF control a 2-DOF piezoelectric actuator equipped with self-measurement," IEEE Rob. Autom. Lett. **3**, 1080–1087 (2018).

[21]Y. Y. Li, L. Cheng, and P. Li, "Modeling and vibration control of a plate coupled with piezoelectric material," Compos. Struct. **62**, 155–162 (2003).

[22]H. Habibullah, H. R. Pota, and I. R. Petersen, "A novel application of minimax LQG control technique for high speed spiral imaging," Asian J. Control **20**, 1400–1412 (2018).

[23]I. R. Petersen and A. Lanzon, "Feedback control of negative-imaginary systems," IEEE Control Syst. **30**, 54–72 (2010).

[24]B. Bhikkaji, S. R. Moheimani, and I. R. Petersen, "A negative imaginary approach to modeling and control of a collocated structure," IEEE/ASME Trans. Mechatronics **17**, 717–727 (2012).

[25]J. Shan, H. T. Liu, and D. Sun, "Slewing and vibration control of a single-link flexible manipulator by positive position feedback (PPF)," Mechatronics **15**, 487–503 (2005).

[26]D. Russell, A. J. Fleming, and S. S. Aphale, "Simultaneous optimization of damping and tracking controller parameters via selective pole placement for enhanced positioning bandwidth of nanopositioners," ASME: J. Dyn. Syst., Meas., Control **137**, 101004 (2015).

[27] L. Li, C. X. Li, G. Gu, and L. M. Zhu, "Positive acceleration, velocity and position feedback based damping control approach for piezo-actuated nanopositioning stages," Mechatronics **47**, 97–104 (2017).

[28] Y. R. Teo, D. Russell, S. S. Aphale, and A. J. Fleming, "Optimal integral force feedback and structured pi tracking control: Application for high speed confocal microscopy," IFAC Proc. Vol. **47**, 11793–11799 (2014).

[29] S. Behrens, A. J. Fleming, and S. R. Moheimani, "Passive vibration control via electromagnetic shunt damping," IEEE/ASME Trans. Mechatronics **10**, 118–122 (2005).

[30] S. R. Moheimani and B. J. Vautier, "Resonant control of structural vibration using charge-driven piezoelectric actuators," IEEE Trans. Control Syst. Technol. **13**, 1021–1035 (2005).

[31] C. X. Li, Y. Ding, G. Y. Gu, and L. M. Zhu, "Damping control of piezo-actuated nanopositioning stages with recursive delayed position feedback," IEEE/ASME Trans. Mechatronics **22**, 855–864 (2017).

[32] B. Bhikkaji and S. R. Moheimani, "Integral resonant control of a piezoelectric tube actuator for fast nanoscale positioning," IEEE/ASME Trans. Mechatronics **13**, 530–537 (2008).

[33] M. Namavar, A. J. Fleming, M. Aleyaasin, K. Nakkeeran, and S. S. Aphale, "An analytical approach to integral resonant control of second-order systems," IEEE/ASME Trans. Mechatronics **19**, 651–659 (2014).

[34] S. S. Aphale, A. J. Fleming, and S. R. Moheimani, "Integral resonant control of collocated smart structures," Smart Mater. Struct. **16**, 439–446 (2007).

[35] A. J. Fleming, S. S. Aphale, and S. O. R. Moheimani, "A new method for robust damping and tracking control of scanning probe microscope positioning stages," IEEE Trans. Nanotechnol. **9**, 438–448 (2010).

[36] E. Pereira, S. S. Aphale, V. Feliu, and S. R. Moheimani, "Integral resonant control for vibration damping and precise tip-positioning of a single-link flexible manipulator," IEEE/ASME Trans. Mechatronics **16**, 232–240 (2011).

[37] E. Al-Mamun, E. Keikha, C. S. Bhatia, and T. H. Lee, "Integral resonant control for suppression of resonance in piezoelectric micro-actuator used in precision servomechanism," Mechatronics **23**, 1–9 (2013).

[38] S. S. Aphale, S. Devasia, and S. R. Moheimani, "High-bandwidth control of a piezoelectric nanopositioning stage in the presence of plant uncertainties," Nanotechnology **19**, 125503 (2008).

[39] S. S. Aphale, A. Ferreira, and S. R. Moheimani, "A robust loop-shaping approach to fast and accurate nanopositioning," Sens. Actuators, A **204**, 88–96 (2013).

[40] K. J. Åström, "Theory and applications of adaptive control–a survey," Automatica **19**, 471–486 (1983).

[41] K. K. Leang and S. Devasia, "Feedback-linearized inverse feedforward for creep, hysteresis, and vibration compensation in AFM piezoactuators," IEEE Trans. Control Syst. Technol. **15**, 927–935 (2007).